Optimal condition to probe strong coupling of two-dimensional excitons and zero-dimensional cavity modes

David Rosser,[1] Dario Gerace,[2] Lucio C. Andreani,[2] and Arka Majumdar[1,3,*]
[1]*Department of Physics, University of Washington, Seattle, Washington 98195, USA*
[2]*Dipartimento di Fisica, Università di Pavia, via Bassi 6, 27100 Pavia, Italy*
[3]*Department of Electrical and Computer Engineering, University of Washington, Seattle, Washington 98195, USA*

(Received 29 June 2021; revised 22 November 2021; accepted 24 November 2021; published 27 December 2021)

The light-matter interaction associated with a two-dimensional excitonic transition coupled to a zero-dimensional photonic cavity is fundamentally different from cavity-coupled localized excitations in quantum dots or color centers, which have negligible spatial extent compared to the cavity-confined mode profile. We provide a succinct expression for calculating the light-matter interaction of a two-dimensional optical transition coupled to a zero-dimensional confined cavity mode. From this expression, we found there is an optimal spatial extent of the excitonic transition that maximizes such an interaction strength due to the competition between minimizing the excitonic envelope function area and maximizing the total integrated field. We also found that at near zero exciton-cavity detuning, the direct transmission efficiency of a waveguide-integrated cavity can be severely suppressed, which suggests performing experiments using a side-coupled cavity.

DOI: 10.1103/PhysRevB.104.235436

I. INTRODUCTION

Realizing single-photon nonlinear optics in a scalable platform could revolutionize both classical and quantum information science and engineering [1–4]. Cavity integrated excitonic materials show great promise among the various systems being explored to reach this strongly nonlinear regime. In general, the light-matter interaction depends on the dimensionality of both excitonic and photonic fields. Quantum confinement of the excitonic wave function yields an increased density of states, which increases the light-matter interaction. This interaction can be further enhanced by integrating the material into a wavelength-scale photonic cavity for temporal and spatial confinement of the electromagnetic field. Furthermore, nonlinearities derived from Coulomb interactions among the charged particles are enhanced due to strong photonic and electronic wave function confinement [5–7], which holds promise for application of these systems as analog quantum simulators [8].

To reach this advantageous nonlinear regime, the cavity mode and the excitonic transition must be strongly coupled, i.e., the coherent coupling strength between the two oscillators should be larger than the system losses. In this regime, the cavity-confined photons and the excitons are hybridized to create a new elementary excitation, known as a polariton, whose properties crucially depend on the dimensionality of the exciton and photon degrees of freedom. Strong coupling and subsequent single photon nonlinear optics have been demonstrated in self-assembled quantum dots coupled to zero-dimensional (0D) cavity systems [9–12]. In a quantum dot, the exciton is confined in all three dimensions, which is defined as a 0D exciton. Similarly, in a photonic crystal defect cavity [13] or a fiber-distributed Bragg reflector (DBR) cavity [14] light is confined at wavelength scale in all three dimensions, making these systems 0D cavities. While such 0D polaritons can provide the strongest nonlinearity, arising from the quantum anharmonicity induced by the 0D exciton [12,15], practical limitations, such as limited range of cavity tuning and the stochastic nature of the position and wavelength of quantum dots, prevent the scalability of such a platform. Another well-studied polaritonic system consists of two-dimensional (2D) excitons in quantum wells integrated with 2D cavities, such as a DBR cavity or nonlocal metasurfaces [16–18]. While many quantum optical effects have been predicted in these 2D exciton-polariton systems [19,20], the lack of excitonic wave function confinement in all three dimensions precluded a clear observation of single photon nonlinearity, i.e., reaching the regime of polariton blockade under resonant excitation [21].

Recently, signatures of single photon nonlinearity have been reported in a III-V quantum well system coupled to an optically confined mode of a curved fiber DBR [22,23]. While these works provide remarkable proof of concept demonstrations with promising perspectives [24], the *in situ* tuning advantage of a fiber-DBR cavity comes at the expense of a larger mode volume as compared to a photonic crystal defect cavity [25,26], as well as an unclear path for scaling to a cavity array. We emphasize that, assuming strong coupling is achieved, a small cavity mode volume is the primary figure of merit for maximizing the optical nonlinearity [27]. As such, on-chip 0D subwavelength mode volume cavities coupled to a 2D excitonic transition can simultaneously provide a large light-matter interaction and a clear path to a scalable architecture. However, strong coupling between such an on-chip 0D cavity mode and 2D exciton has not yet been demonstrated.

*Corresponding author: arka@uw.edu

A primary difficulty to achieve such an accomplishment is the inevitable deterioration of quantum well excitons due to etching, when inorganic semiconductor material platforms are used. This problem can be alleviated by using atomically thin van der Waals materials, such as transition metal dichalcogenides (TMD), as they can be transferred on a prefabricated photonic crystal cavity. However, even though these materials have long been integrated with 0D on-chip photonic crystal defect cavities [28,29], to date there has been no report on light-matter strong coupling beyond the dispersive coupling results observed recently at large exciton-cavity detunings [30,31].

In this work, we theoretically analyze such a system to elucidate the conditions for experimentally probing the strong coupling regime between 2D excitons and the 0D cavity mode of a subwavelength photonic nanocavity. More specifically, we considered the neutral exciton in a monolayer TMD, such as $MoSe_2$, deposited on a silicon nitride, in-line photonic crystal defect cavity as a model system to be quantitatively analyzed. We have numerically calculated the light-matter interaction strength depending on the specific near field profile of the confined mode. We show that there is an optimal spatial coverage of the 2D exciton in such a 0D cavity where the light-matter interaction is maximized. Additionally, applying an input-output approach to calculate the cavity transmission, we show that due to the absorption from 2D material the cavity transmission drops significantly for a resonant exciton-cavity system. By exploiting side coupling between a waveguide and the cavity containing the excitonic material, strong coupling could be probed in a transmission configuration. The theoretical estimate of the light-matter interaction and manifestation of significant transmission suppression agree well with experiments reported on this system [30].

II. THEORETICAL MODEL

The Hamiltonian describing the in-line, single-mode cavity and the excitonic mode as two coupled oscillators is (in a frame rotating at the frequency of an external driving laser) [32,33]

$$H_{XC} = \hbar\Delta_{XL}\hat{a}^\dagger\hat{a} + \hbar\Delta_{CL}\hat{c}^\dagger\hat{c} + \hbar g(\hat{a}^\dagger\hat{c} + \hat{c}^\dagger\hat{a}) + i\hbar\sqrt{\gamma_1}(\alpha\hat{c}^\dagger + \alpha^*\hat{c}), \quad (1)$$

with a light-matter interaction strength g, where $\Delta_{XL} = \omega_X - \omega_L$ and $\Delta_{CL} = \omega_C - \omega_L$ are the detunings of the excitonic transition (ω_X) and cavity mode (ω_C) from the laser frequency (ω_L), respectively; $\hat{a}$ ($\hat{c}$) is the bosonic annihilation operator for the exciton (cavity) mode. γ_1 is the input coupling to the cavity and $|\alpha|^2$ is the incident photon flux for a coherent, classical cavity drive. We are only concerned with the exciton mode with the same spatial wave function as the cavity mode due to the limited dispersion of a 0D cavity [6,21]. Hence, we neglect the in-plane momentum distribution of the 2D exciton in our model.

We estimate the light-matter interaction strength g between the 2D exciton and the 0D cavity by noting that the dielectric function of monolayer $MoSe_2$ can be modeled as a Lorentzian oscillator $\varepsilon(\omega) = \varepsilon_b + \frac{A}{\omega_X^2 - \omega^2 - i\gamma_X\omega}$ [34], where $\varepsilon_b = 26$ is the background dielectric constant of the TMD layer [35], which

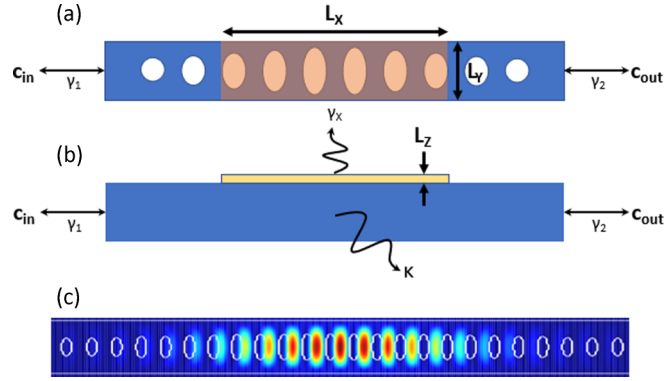

FIG. 1. (a) Top-view pictorial representation of a photonic crystal defect cavity embedded in line to a waveguide, coupled to a quantum well supporting a two-dimensional excitonic transition. Blue is the confining dielectric and orange is the quantum well. $\gamma_{1,2}$ are the waveguide-coupled losses. L_x is the length of the integrated quantum well. L_y is the width of the integrated quantum well. (b) Side view of the waveguide. κ and γ_X are the intrinsic losses of the cavity and exciton, respectively. L_z is the effective height of the integrated quantum well. (c) Electric field intensity simulated at the center of a silicon nitride nanobeam cavity by a finite-difference time-domain electromagnetic solver at the cavity mode resonant frequency, showing wavelength scale field confinement. The maximum field intensity is seen in the center of the nanobeam.

results in a perturbative shift of the cavity resonance; A is an "effective" oscillator strength having dimensions of a squared energy, ω_X is the energy of the excitonic transition (with $\hbar = 1$), and γ_X is the total exciton loss rate (including both radiative and nonradiative contributions). In the following, we fix $A = 0.4$ eV^2 as a representative value from experimental reflectivity measurements [34]. By treating the monolayer TMD as a delocalized semiconductor quantum well exciton in a dielectric medium coupled to a confined optical mode of the cavity a concise expression for the light-matter interaction energy can be derived (Appendix A):

$$\hbar g = \frac{\sqrt{A}}{2}\sqrt{\frac{L_z}{L_{\text{eff}}}}. \quad (2)$$

A is the effective oscillator strength contained in the dielectric constant, L_z is the thickness of the monolayer material, and L_{eff} is a length scale defined by the competition between minimizing the excitonic envelope function area and maximizing the total integrated field:

$$L_{\text{eff}} = \left(\frac{1}{L_x L_y}\int_0^{L_x} dx \int_0^{L_y} dy\left[\mathbf{E}^{(2D)}_{\text{norm},x}(x,y) + \mathbf{E}^{(2D)}_{\text{norm},y}(x,y)\right]\right)^{-2}. \quad (3)$$

L_x (L_y) is the length (width) of the integrated monolayer material [Fig. 1(b)] and $\mathbf{E}^{(2D)}_{\text{norm},x}$ ($\mathbf{E}^{(2D)}_{\text{norm},y}$) is the normalized electromagnetic field in the x (y) direction.

While this formalism can be applied to any extended 2D coherent media in confined cavity geometries, we illustrate this result assuming parameters appropriate for a $MoSe_2$ monolayer deposited on a silicon nitride in-line nanobeam cavity, because such a system can be readily fabricated in practice [30]. Using a finite difference time domain (FDTD)

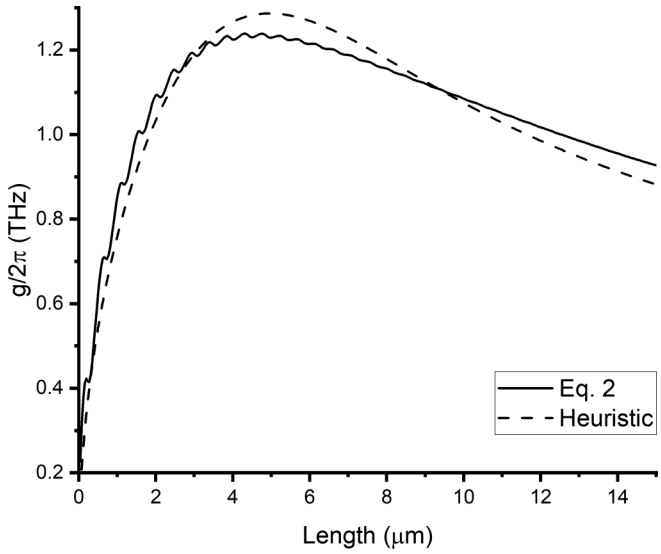

FIG. 2. Light-matter interaction for different lengths L_x of the integrated quantum well with L_y fixed to the width of the waveguide. The oscillations seen in the light-matter interaction originate from the periodic variation of the electric field commensurate with the lattice spacing of the nanobeam air holes. $g/2\pi = 1.2389$ THz is the maximum value for this cavity design and oscillator strength. The dotted line is a fit to the heuristic equation in the main text elucidating the peak in the light-matter interaction for a cavity confinement length of $\sigma = 1.77\mu$m.

electromagnetic solver (from Lumerical-Ansys), we calculate the cavity field profile [Fig. 1(b)] to be used into Eq. (3) with a resonance at $\omega_C/2\pi = 395.777$ THz ($\lambda_C = 757$ nm, Appendix B). Taking the effective thickness of the monolayer material to be equal to the measured thickness, $L_z \equiv 0.7$ nm, we find a maximal value for the light-matter interaction with monolayer length $L_x = 4.31\mu$m (Fig. 2). This result runs counter to the result associated with the Dicke model, in which a giant oscillator is expected to grow monotonically with the number of oscillators ($g \propto \sqrt{N} g_0$) [36], which in this case correlates to the area of monolayer $MoSe_2$ assuming the excitonic wave function is delocalized over the entire field integration region. For a confined field in the cavity we would then expect the light-matter interaction strength g to saturate with the length of the monolayer material and not have a nonmonotonic behavior as shown in Fig. 2. Note that we experimentally observed a light-matter interaction commensurate with our theoretical estimate [30].

Heuristically, we can understand this optimal overlap between the 2D exciton envelope function and the cavity field profile in terms of the light-matter interaction by recognizing that the steady state electric field of the nanobeam cavity has an approximately Gaussian envelope along the cavity axis, with a width σ (units of length) modulated by a sinusoidal signal of the photonic lattice periodicity [37] [e.g., Fig. 1(c)]. Assuming the length of the coherent polarization due to the delocalized excitonic wave function is the same as the length of the cavity integration, L_x, substitution of a Gaussian cavity field profile into Eq. (3) gives a light-matter interaction strength of the form $g \propto \frac{1}{\sqrt{L_x}} \int_{-L_x/2}^{L_x/2} e^{-\frac{1}{2}(\frac{x}{\sigma})^2} dx \propto \frac{\sigma}{\sqrt{L_x}} \mathrm{erf}(\frac{L_x}{2\sqrt{2}\sigma})$. The latter function gives a peak in the light-matter interaction strength $L_x \sim 2.80\sigma$, which roughly corresponds to $L_x = 2.44\sigma$ that is numerically calculated for the designed in-line nanobeam cavity. For the sake of clarity and completeness, we overlay this estimate on top of the numerical simulation in Fig. 2.

We now discuss the experimental scheme allowing us to probe these polaritons. Often, such light-matter coupled systems are measured via incoherent photoluminescence. However, coherent driving in the transmission configuration is necessary in view of practical development of quantum technology applications [38]. For the on-chip configuration, the exciton-polariton modes are generally probed using a two-sided cavity [39] [Fig. 1(a)]. An input grating is used to send light to the coupled system and the transmitted light is collected via an output grating [30]. Using the input-output formalism [40] an analytic transmission function for the system described by the Hamiltonian in Eq. (1) can be derived (Appendix C):

$$T(\omega) = \frac{\gamma_1 \gamma_2}{\left[\omega - \omega_C - \frac{(\omega-\omega_X)g^2}{(\omega-\omega_X)^2+\gamma_X^2}\right]^2 + \left[\kappa + \frac{1}{2}(\gamma_1+\gamma_2) + \frac{\gamma_X g^2}{(\omega-\omega_X)^2+\gamma_X^2}\right]^2}. \quad (4)$$

We include intrinsic cavity losses κ, cavity coupling to the input (output) waveguide $\gamma_1(\gamma_2)$, and excitonic losses γ_X. In our model system, the in-line nanobeam cavity is symmetrically coupled to the waveguide (i.e., $\gamma = \gamma_1 = \gamma_2$).

The intrinsic cavity loss and cavity-waveguide coupling can be inferred from the FDTD simulations. The designed in-line nanobeam cavity has a loaded quality factor $Q_{\mathrm{loaded}} = 11\,924$ and an intrinsic quality factor $Q_{\mathrm{intrinsic}} = 25\,480$. The intrinsic quality factor of the cavity is found by increasing the number of Bragg mirror holes until the waveguide is no longer coupled to the cavity and the simulated quality factor approaches an asymptotic value. We note that, for this particular cavity, we are choosing an on-substrate, silicon nitride, in-line, nanobeam cavity due to its mechanical stability [26], hence the reduced quality factor compared to a suspended nanobeam cavity. The decay rate of the cavity field is $\kappa = \frac{1}{2}\frac{\omega_C}{Q_{\mathrm{intrinsic}}} = 2\pi \times 7.77$ GHz. Similarly, the decay rate of the loaded cavity field is $\kappa + \gamma = \frac{1}{2}\frac{\omega_C}{Q_{\mathrm{loaded}}} = 2\pi \times 16.6$ GHz, which gives a waveguide-coupled field decay rate $\gamma = 2\pi \times 8.83$ GHz. This results in an estimated maximum transmission efficiency $T_{\max} = (\frac{\gamma}{\kappa+\gamma})^2 = 0.28$ [41].

To probe the system in the strong coupling regime we need to calculate the transmission efficiency for a resonant exciton-cavity system. The temperature-dependent excitonic loss can be approximated using the Rudin equation $\gamma_X(T) = \frac{1}{2}[\gamma_0 + c_1 T + \frac{c_2}{e^{\Omega/k_B T}-1}]$, where γ_0 is the intrinsic linewidth, c_1 includes exciton interactions with acoustic phonons, c_2 includes exciton interactions with longitudinal-optical phonons,

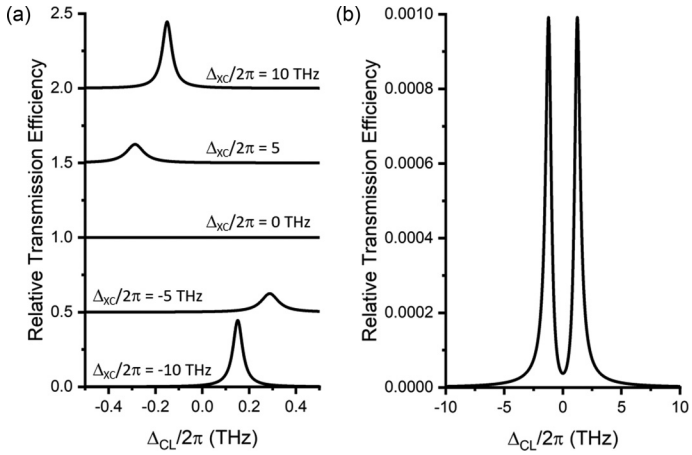

FIG. 3. (a) Transmission spectrum relative to $T_{\max}$ [$T_{\text{relative}} = T(\omega)/T_{\max}$] at different exciton-cavity detunings Δ_{XC}. $\Delta_{CL} = \omega_C - \omega_L$ is the laser detuning from the bare cavity resonance. For clarity, the transmission spectrum are offset by 0.5 from the lower to upper plots. (b) Transmission spectrum relative to $T_{\max}$ at zero exciton-cavity detuning. The solid line in panel (b) is the magnified middle line of panel (a) corresponding to $\Delta_{XC} = 0$. Note the different x-axis range. Parameters: $\kappa/2\pi = 7.77$ GHz, $\gamma/2\pi = 8.83$ GHz, $\gamma_X/2\pi = 566$ GHz, and $g/2\pi = 1.2389$ THz.

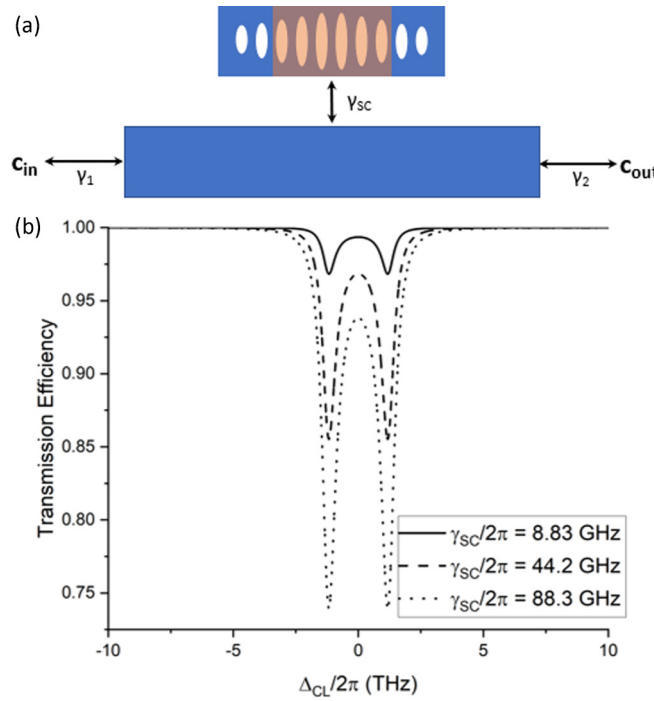

FIG. 4. (a) Top-view pictorial representation of a photonic crystal defect cavity side coupled to a waveguide, coupled to a quantum well supporting a two-dimensional excitonic transition. Blue is the confining dielectric and orange is the quantum well. γ_{SC} is the waveguide-coupled loss for the side-coupled cavity. (b) Side-coupled transmission spectrum for increasing values of the waveguide-coupled loss. Parameters: $\kappa/2\pi = 7.77$ GHz, $\gamma_X/2\pi = 566$ GHz, and $g/2\pi = 1.2389$ THz.

and Ω is the average phonon energy [42]. We fix $\hbar\gamma_0 = 4.3$ meV, $c_1 = 91\ \mu\text{eVK}^{-1}$, $c_2 = 15.6$ meV, and $\Omega = 30$ meV as representative values for unencapsulated monolayer $MoSe_2$ [43]. We assume $\gamma_X = 2\pi \times 566$ GHz at the temperature $T = 4.2$ K, as a representative value for the excitonic linewidth in the strong coupling regime.

With these values we calculate the transmission spectrum of the coupled exciton-cavity system [Fig. 3(a)]. At large exciton-cavity detuning the transmission efficiency approaches the bare cavity value $T_{\max}$. At smaller detunings, the dispersive cavity shift is noticeable with broadening of the transmission peak. Near zero detuning, however, the intensity of the transmission peak in the strong coupling regime is several orders of magnitude smaller than the bare cavity transmission [Fig. 3(b)]. Substituting the parameters, for example, from Fig. 3 into Eq. (C16) we find the maximum transmission efficiency with the integrated 2D exciton relative to the bare cavity transmission maximum is only 0.098%. Thus a major drawback of an in-line symmetric two-sided cavity is the drastic suppression of transmission near zero exciton-cavity detuning. Note that we experimentally observed a similar reduction in cavity transmission in our exciton-cavity system [30].

The drastic reduction in the transmission efficiency of an in-line cavity primarily comes from the large excitonic loss rate γ_X. To ensure an appreciable transmission efficiency, the waveguide-cavity coupling rate (γ) can be increased. But this will reduce the quality factor of the cavity and reaching the strong coupling regime may not be possible. The difficulty of demonstrating high transmission efficiency of the cavity mode near zero exciton-cavity detuning stems from the mismatch between the loss of the hybridized polariton mode and waveguide-coupled loss [44,45]. This effect is similar to the condition of reaching critical coupling in a waveguide-coupled microring resonator [46]. One way to circumvent this loss in transmission will be to employ a side-coupled waveguide-cavity system [47]. By engineering the side-coupled, waveguide-cavity coupling rate (γ_{SC}) the radiative loss of the polariton can be kept relatively low while still maintaining sufficient waveguide coupling to observe polariton modes in transmission.

In a side-coupled nanobeam cavity, by modifying the width and the gap of the coupled waveguide to the nanobeam cavity the waveguide-coupled loss can be engineered. Such side-coupled geometry partially decouples the intrinsic cavity quality factor and field profile from the transmission properties of the cavity. We analyzed the performance of such a side-coupled cavity and found that sufficient transmission contrast can be achieved in the strong coupling regime [Appendix C, Fig. 4(a)]. Reaching critical coupling in the side-coupled cavity design requires the waveguide-cavity coupling rate to be the same as the polariton loss, which is necessarily no longer in the strong coupling regime. However, in the under-coupled regime, by carefully choosing the waveguide-cavity coupling rate we can achieve a measurable transmission contrast, as we verified numerically [Fig. 4(b)]. The side-coupled, waveguide-cavity coupling rate (γ_{SC}) essentially provides an additional degree of freedom for cavity design that is absent in in-line cavities.

III. DISCUSSION

We have estimated an optimal length of monolayer $MoSe_2$ for the integration onto a nanobeam cavity. The successful study of polariton physics in this material platform will likely require *ex situ* etching due to the size of the monolayer and positional accuracy [48]. Despite the improved cooperativity ($C = \frac{g^2}{\gamma_X(\kappa+\gamma)}$) found by maximizing the light-matter interaction, the small transmission efficiency remains a challenge to experimentally probe the strong coupling regime [30]. This low transmission efficiency may be avoided by decoupling the waveguide-coupled loss from the intrinsic cavity loss, using a side-coupled nanobeam or ring resonator [41,47]. This allows for an extra degree of freedom to increase the waveguide-coupled loss at a similar rate to that of the cavity broadening from the perturbing monolayer $MoSe_2$. The limiting factor in this system is the linewidth of the neutral exciton in monolayer $MoSe_2$. Hexagonal boron nitride encapsulation is a means to narrow the linewidth by modifying the dielectric environment and reducing sample inhomogeneity [49]. However, experiment may be better served by pursuing two-dimensional excitonic transitions with intrinsically narrow linewidths [50].

ACKNOWLEDGMENTS

The research was supported by Grants No. NSF-1845009 and No. NSF-ECCS-1708579. D.R. is partially supported by a Clean Energy Institute graduate fellowship. D.G. acknowledges support from the Italian Ministry of University (MUR) through the PRIN project "Interacting Photons in Polariton Circuits" – INPhoPOL (Grant No. 2017P9FJBS).

APPENDIX A: LIGHT-MATTER INTERACTION

The light-matter interaction in the dipole approximation for an excitonic transition in a quantum well (QW) can be written [6,32,51,52]

$$\hbar g = \left(\frac{\hbar^2 e^2}{4\varepsilon_0 m_0} f_{xy}\right)^{1/2} \int_\Sigma dx\, dy\, \hat{\mathbf{d}} \cdot \mathbf{E}^{2D}_{\text{norm}}(x,y) F_{\text{exc}}(x,y), \tag{A1}$$

where $\hbar$ is the reduced Planck constant, e is the charge of an electron, ϵ_o is the vacuum permittivity, f_{xy} is an oscillator strength per unit area, m_0 is the free electron mass, $\hat{\mathbf{d}}$ is a unit vector pointing primarily in the plane of the quantum well, $\mathbf{E}^{2D}_{\text{norm}}$ is the normalized electric field at the surface of the nanobeam cavity, and F_{exc} is the normalized exciton envelope function. The integration is performed over the whole cavity region.

We choose to normalize the electric field such that $\mathbf{E}^{2D}_{\text{norm}}(x,y) = \frac{1}{\sqrt{\mathcal{N}}}\mathbf{E}(x,y,z_{QW})$ and $\mathcal{N} = \int \varepsilon(\mathbf{r})|\mathbf{E}(\mathbf{r})|^2$. z_{QW} is the z coordinate of the 2D exciton and $\mathbf{E}(x,y,z)$ is the electric field calculated by a FDTD electromagnetic solver at the cavity mode resonant frequency. The normalized exciton envelope function is defined as $F_{\text{exc}} = 1/\sqrt{S}$, where S is the effective area of the excitonic transition, which we take to be the physical area of the monolayer material $S = L_x L_y$, assuming the excitonic wave function is delocalized over the whole monolayer area. These definitions lead to the effective length scale of Eq. (3).

An equivalent expression for the dielectric function of a quantum well is [53]

$$\varepsilon(\omega) = \varepsilon_b\left(1 + \frac{E_L^2 - E_X^2}{E_X^2 - (\hbar\omega)^2 - i\hbar^2\gamma_X\omega}\right) \tag{A2}$$

$$\simeq \varepsilon_b\left(1 + \frac{2E_{LT}E_X}{E_X^2 - (\hbar\omega)^2 - i\hbar^2\gamma_X\omega}\right), \tag{A3}$$

where $E_{LT} = \hbar^2 e^2/(2\varepsilon_0\varepsilon_b m_0 E_X L_z)$ is the longitudinal-transverse splitting. L_z is an effective thickness that accounts for the finite penetration of the exciton envelope function into the barriers of the quantum well. The oscillator strength per unit area can then be determined from the oscillator strength measured from reflectivity measurements ($f_{xy} = \frac{\varepsilon_0 m_0 L_z}{\hbar^2 e^2} A$, where A is defined in the main text as the effective oscillator strength in the Lorentz oscillator expression) [34]. The compact expression for the light-matter interaction in Eq. (2) follows from substitution of this result into Eq. (A1) with the definition of L_{eff}.

APPENDIX B: CAVITY EXAMPLE

A photonic crystal nanobeam cavity is chosen for its large quality factor, small mode volume, and high on-resonance transmission efficiency [37]. We emphasize that the formalism presented in this paper can be used for any other cavities. However, to calculate the light-matter interaction strength we need to use the cavity field profile of a specific cavity design. The one-dimensional photonic crystal defect cavity, also known as a nanobeam cavity, is made of a $t_{\text{waveguide}} = 220$ nm thick and $w_{\text{waveguide}} = 779$ nm wide silicon nitride film on silicon oxide substrate. From the center of the nanobeam, where the light is confined, there are 10 tapering holes and 20 Bragg mirror holes. All of the holes are elliptical with a minor axis radius fixed to 40 nm. The tapering holes begin with a 178 nm major axis diameter and a 215 nm center-to-center distance. The tapering region is quadratically tapered to a 121 nm major axis radius and a 233 nm center-to-center distance. The Bragg mirror region has a major axis radius fixed to 121 nm and a 233 nm center-to-center distance. The performance of the nanobeam cavity was optimized using Lumerical's finite-difference time-domain (FDTD) electromagnetic solver. The dimensions are identical to the cavity found in an experimental dispersive coupling result [30].

APPENDIX C: INPUT-OUTPUT THEORY

Following the input-output theory of Collett and Gardiner [39], for a single-mode, in-line cavity the quantum Langevin equations describing the internal cavity and excitonic modes with a single external driving field are

$$\frac{d\hat{c}}{dt} = -\frac{i}{\hbar}[\hat{c}, \hat{H}_{XC}] - \frac{\gamma_1}{2}\hat{c} - \frac{\gamma_2}{2}\hat{c} + \sqrt{\gamma_1}\hat{c}_{\text{in}}, \tag{C1}$$

$$\frac{d\hat{a}}{dt} = -\frac{i}{\hbar}[\hat{a}, \hat{H}_{XC}]. \tag{C2}$$

$\hat{H}_{XC} = \hbar\tilde{\Delta}_{XL}\hat{a}^\dagger\hat{a} + \hbar\tilde{\Delta}_{CL}\hat{c}^\dagger\hat{c} + \hbar g(\hat{a}^\dagger\hat{c} + \hat{c}^\dagger\hat{a})$ is the Hamiltonian described in Eq. (1),except $\tilde{\Delta}_{CL} = (\omega_C - \omega_L) - i\kappa$ and $\tilde{\Delta}_{XL} = (\omega_X - \omega_L) - i\gamma_X$ are the detunings and intrinsic radiative loss of the resonator mode (ω_C, κ) and excitonic transition

(ω_X, γ_X) from the laser frequency (ω_L), respectively. $\gamma_{1,2}$ are the cavity damping constants for the two sides of the cavity. $\hat{c}_{\text{in}}$ is the external driving field coupled to the cavity through γ_1. The transmitted field $\hat{c}_{\text{out}}$ is coupled to the cavity via γ_2, as described by the equation

$$\hat{c}_{\text{out}} = \sqrt{\gamma_2}\hat{c}. \tag{C3}$$

Inserting Eq. (1) into Eq. (C1) and Eq. (C2), and then computing the commutator gives

$$\frac{d\hat{c}}{dt} = -i\tilde{\omega}_{CL}\hat{c} - ig\hat{a} - \frac{\gamma_1}{2}\hat{c} - \frac{\gamma_2}{2}\hat{c} + \sqrt{\gamma_1}\hat{c}_{\text{in}} + \sqrt{\gamma_1}\alpha, \tag{C4}$$

$$\frac{d\hat{a}}{dt} = -i\tilde{\omega}_{XL}\hat{a} - ig\hat{c}. \tag{C5}$$

In the frequency domain the internal mode operator is taken to be

$$\tilde{c}(\omega) = \frac{1}{\sqrt{2\pi}}\int_{-\infty}^{\infty} e^{i\omega t}\hat{c}(t)dt \tag{C6}$$

and the excitonic mode operator is

$$\tilde{a}(\omega) = \frac{1}{\sqrt{2\pi}}\int_{-\infty}^{\infty} e^{i\omega t}\hat{a}(t)dt. \tag{C7}$$

Equations (C4) and (C5) in the frequency domain are then

$$-i\omega\tilde{c} = -i\tilde{\omega}_C\tilde{c} - ig\tilde{a} - \frac{\gamma_1}{2}\tilde{c} - \frac{\gamma_2}{2}\tilde{c} + \sqrt{\gamma_1}\tilde{c}_{\text{in}}, \tag{C8}$$

$$-i\omega\tilde{a} = -i\tilde{\omega}_X\tilde{a} - ig\tilde{c}. \tag{C9}$$

For observations of the vacuum Rabi splitting we assume a weak incident field with $\alpha \to 0$. Equation (C9) can be solved for $\tilde{a}$ in terms of $\tilde{c}$. This result can be substituted into Eq. (C8), which can then be solved for $\tilde{c}$ in terms of $\tilde{c}_{\text{in}}$. Finally, this result can be substituted into Eq. (C3). The transmission spectrum in the frequency domain for an in-line cavity is then

$$T(\omega) = \left|\frac{\tilde{c}_{\text{out}}}{\tilde{c}_{\text{in}}}\right|^2 \tag{C10}$$

$$= \left|\frac{\sqrt{\gamma_1\gamma_2}}{-i(\omega - \tilde{\omega}_C) + \frac{1}{2}(\gamma_1+\gamma_2) + \frac{g^2}{-i(\omega-\tilde{\omega}_X)}}\right|^2. \tag{C11}$$

Collecting real and imaginary components of the expression we have

$$T(\omega) = \left|\frac{\sqrt{\gamma_1\gamma_2}}{-i\left[(\omega-\omega_C) - \frac{(\omega-\omega_X)g^2}{(\omega-\omega_X)^2+\gamma_X^2}\right] + \left[\frac{1}{2}(\gamma_1+\gamma_2) + \kappa + \frac{\gamma_X g^2}{(\omega-\omega_X)^2+\gamma_X^2}\right]}\right|^2. \tag{C12}$$

The transmitted spectrum is then

$$T(\omega) = \frac{\gamma_1\gamma_2}{\left[\omega - \omega_C - \frac{(\omega-\omega_X)g^2}{(\omega-\omega_X)^2+\gamma_X^2}\right]^2 + \left[\kappa + \frac{1}{2}(\gamma_1+\gamma_2) + \frac{\gamma_X g^2}{(\omega-\omega_X)^2+\gamma_X^2}\right]^2}. \tag{C13}$$

This is the result reported in Eq. (4). For an in-line resonator symmetrically coupled to the waveguide ($\gamma = \gamma_1 = \gamma_2$), the transmitted spectrum of the exciton-resonator system reduces to

$$T(\omega) = \frac{\gamma^2}{\left[\omega - \omega_C - \frac{(\omega-\omega_X)g^2}{(\omega-\omega_X)^2+\gamma_X^2}\right]^2 + \left[\kappa + \gamma + \frac{\gamma_X g^2}{(\omega-\omega_X)^2+\gamma_X^2}\right]^2}. \tag{C14}$$

The minima for Eq. (C14) in the strong coupling regime at zero exciton-cavity detuning (setting $\omega = \omega_C = \omega_X$) gives a transmission of

$$T = \left(\frac{\gamma}{\kappa+\gamma}\right)^2 \frac{1}{(1+C)^2}, \tag{C15}$$

where we define the cooperativity as $C \equiv \frac{g^2}{\gamma_X(\kappa+\gamma)}$, which effectively quantifies the visibility of the polariton modes. In the absence of an optical transition this reduces to the $T_{\max}$ discussed in the main article.

At zero exciton-cavity detuning ($\omega_C = \omega_X$) by setting the derivative of Eq. (C14) equal to zero ($\frac{dT}{d\omega} = 0$) we find maxima at $\omega_\pm = \omega_C \pm \sqrt{C'g^2 - \gamma_X^2}$ associated with normal mode splitting in the strong coupling regime. Substituting $\omega_\pm$ into Eq. (C14), the peaks have an analytic expression

$$T(\omega_\pm) = \frac{\gamma^2 C'}{g^2(C'-1)^2 + [(\kappa+\gamma)^2 - \gamma_X^2]C' + 2\gamma_X[(\kappa+\gamma)+\gamma_X]}, \tag{C16}$$

where we define $C' = \sqrt{1 + \frac{2}{C}[1 + \gamma_X/(\kappa+\gamma)]}$.

For a single-mode, side-coupled resonator the quantum Langevin equations describing the internal cavity and excitonic modes with a single external driving field are [54,55]

$$\frac{d\hat{c}}{dt} = -\frac{i}{\hbar}[\hat{c}, \hat{H}_{XC}] - i\sqrt{\gamma_{SC}}\hat{c}_{\text{in}}, \tag{C17}$$

$$\frac{d\hat{a}}{dt} = -\frac{i}{\hbar}[\hat{a}, \hat{H}_{XC}]. \tag{C18}$$

The transmitted field $\hat{c}_{\text{out}}$ is coupled to the resonator via γ_{SC}, as described by the equation

$$\hat{c}_{\text{out}} = \hat{c}_{\text{in}} - i\sqrt{\gamma_{SC}}\hat{c}. \tag{C19}$$

The transmission spectrum for the side-coupled cavity can then be similarly derived to be

$$T(\omega) = \left|\frac{\tilde{c}_{\text{out}}}{\tilde{c}_{\text{in}}}\right|^2 = \left|1 - \frac{i\gamma_{SC}(\omega - \tilde{\omega}_X)}{(\omega - \tilde{\omega}_C)(\omega - \tilde{\omega}_X) - g^2}\right|^2. \tag{C20}$$

Here, $\tilde{\omega}_C = \omega_C - i(\kappa + \gamma_{SC})$ and γ_{SC} is the coupling rate between the waveguide and the cavity.

[1] D. E. Chang, A. S. Sørensen, E. A. Demler, and M. D. Lukin, Nat. Phys. **3**, 807 (2007).
[2] D. Englund, A. Majumdar, M. Bajcsy, A. Faraon, P. Petroff, and J. Vučković, Phys. Rev. Lett. **108**, 093604 (2012).
[3] D. A. B. Miller, J. Lightwave Technol., JLT **35**, 346 (2017).
[4] S. Sun, H. Kim, Z. Luo, G. S. Solomon, and E. Waks, Science **361**, 57 (2018).
[5] I. Carusotto and C. Ciuti, Rev. Mod. Phys. **85**, 299 (2013).
[6] E. V. Denning, M. Wubs, N. Stenger, J. Mork, and P. T. Kristensen, arXiv:2103.14488.
[7] E. V. Denning, M. Wubs, N. Stenger, J. Mork, and P. T. Kristensen, arXiv:2103.14484.
[8] *Quantum Simulations with Photons and Polaritons: Merging Quantum Optics with Condensed Matter Physics*, edited by D. G. Angelakis, Quantum Science and Technology (Springer International Publishing, Berlin, 2017).
[9] A. Faraon, I. Fushman, D. Englund, N. Stoltz, P. Petroff, and J. Vučković, Nat. Phys. **4**, 859 (2008).
[10] A. Majumdar, M. Bajcsy, and J. Vučković, Phys. Rev. A **85**, 041801(R) (2012).
[11] A. Reinhard, T. Volz, M. Winger, A. Badolato, K. J. Hennessy, E. L. Hu, and A. Imamoğlu, Nat. Photon. **6**, 93 (2012).
[12] D. Najer, I. Söllner, P. Sekatski, V. Dolique, M. C. Löbl, D. Riedel, R. Schott, S. Starosielec, S. R. Valentin, A. D. Wieck, N. Sangouard, A. Ludwig, and R. J. Warburton, Nature (London) **575**, 622 (2019).
[13] M. Notomi, Rep. Prog. Phys. **73**, 096501 (2010).
[14] D. Hunger, T. Steinmetz, Y. Colombe, C. Deutsch, T. W. Hänsch, and J. Reichel, New J. Phys. **12**, 065038 (2010).
[15] K. Hennessy, A. Badolato, M. Winger, D. Gerace, M. Atatüre, S. Gulde, S. Fält, E. L. Hu, and A. Imamoğlu, Nature (London) **445**, 896 (2007).
[16] T. Byrnes, N. Y. Kim, and Y. Yamamoto, Nat. Phys. **10**, 803 (2014).
[17] X. Liu, T. Galfsky, Z. Sun, F. Xia, E.-c. Lin, Y.-H. Lee, S. Kéna-Cohen, and V. M. Menon, Nat. Photon. **9**, 30 (2015).
[18] Y. Chen, S. Miao, T. Wang, D. Zhong, A. Saxena, C. Chow, J. Whitehead, D. Gerace, X. Xu, S.-F. Shi, and A. Majumdar, Nano Lett. **20**, 5292 (2020).
[19] D. Gerace, H. E. Türeci, A. Imamoglu, V. Giovannetti, and R. Fazio, Nat. Phys. **5**, 281 (2009).
[20] T. C. H. Liew and V. Savona, Phys. Rev. Lett. **104**, 183601 (2010).
[21] A. Verger, C. Ciuti, and I. Carusotto, Phys. Rev. B **73**, 193306 (2006).
[22] A. Delteil, T. Fink, A. Schade, S. Höfling, C. Schneider, and A. İmamoğlu, Nat. Mater. **18**, 219 (2019).
[23] G. Muñoz-Matutano, A. Wood, M. Johnsson, X. Vidal, B. Q. Baragiola, A. Reinhard, A. Lemaître, J. Bloch, A. Amo, G. Nogues, B. Besga, M. Richard, and T. Volz, Nat. Mater. **18**, 213 (2019).
[24] D. Gerace, F. Laussy, and D. Sanvitto, Nat. Mater. **18**, 200 (2019).
[25] L. Greuter, S. Starosielec, D. Najer, A. Ludwig, L. Duempelmann, D. Rohner, and R. J. Warburton, Appl. Phys. Lett. **105**, 121105 (2014).
[26] T. K. Fryett, Y. Chen, J. Whitehead, Z. M. Peycke, X. Xu, and A. Majumdar, ACS Photon. **5**, 2176 (2018).
[27] S. Ferretti and D. Gerace, Phys. Rev. B **85**, 033303 (2012).
[28] X. Gan, Y. Gao, K. Fai Mak, X. Yao, R.-J. Shiue, A. van der Zande, M. E. Trusheim, F. Hatami, T. F. Heinz, J. Hone, and D. Englund, Appl. Phys. Lett. **103**, 181119 (2013).
[29] S. Wu, S. Buckley, A. M. Jones, J. S. Ross, N. J. Ghimire, J. Yan, D. G. Mandrus, W. Yao, F. Hatami, J. Vučković, A. Majumdar, and X. Xu, 2D Mater. **1**, 011001 (2014).
[30] D. Rosser, D. Gerace, Y. Chen, Y. Liu, J. Whitehead, A. Ryou, L. C. Andreani, and A. Majumdar, Opt. Mater. Express **12**, 59 (2022).
[31] C. Qian, V. Villafañe, P. Soubelet, A. Hötger, T. Taniguchi, K. Watanabe, N. P. Wilson, A. V. Stier, A. W. Holleitner, and J. J. Finley, arXiv:2107.04387.
[32] D. Gerace and L. C. Andreani, Phys. Rev. B **75**, 235325 (2007).
[33] H. Deng, H. Haug, and Y. Yamamoto, Rev. Mod. Phys. **82**, 1489 (2010).
[34] N. Lundt, A. Maryński, E. Cherotchenko, A. Pant, X. Fan, S. Tongay, G. Sęk, A. V. Kavokin, S. Höfling, and C. Schneider, 2D Mater. **4**, 015006 (2016).
[35] Y. V. Morozov and M. Kuno, Appl. Phys. Lett. **107**, 083103 (2015).
[36] B. M. Garraway, Philos. Trans. R. Soc. A **369**, 1137 (2011).
[37] Q. Quan and M. Loncar, Opt. Express, OE **19**, 18529 (2011).
[38] D. Englund, A. Majumdar, A. Faraon, M. Toishi, N. Stoltz, P. Petroff, and J. Vučković, Phys. Rev. Lett. **104**, 073904 (2010).

[39] M. J. Collett and C. W. Gardiner, Phys. Rev. A **30**, 1386 (1984).
[40] C. W. Gardiner and M. J. Collett, Phys. Rev. A **31**, 3761 (1985).
[41] Y. Xu, Y. Li, R. K. Lee, and A. Yariv, Phys. Rev. E **62**, 7389 (2000).
[42] S. Rudin, T. L. Reinecke, and B. Segall, Phys. Rev. B **42**, 11218 (1990).
[43] M. Selig, G. Berghäuser, A. Raja, P. Nagler, C. Schüller, T. F. Heinz, T. Korn, A. Chernikov, E. Malic, and A. Knorr, Nat. Commun. **7**, 13279 (2016).
[44] J.-T. Shen and S. Fan, Phys. Rev. A **79**, 023838 (2009).
[45] J.-T. Shen and S. Fan, Phys. Rev. A **79**, 023837 (2009).
[46] S. L. Chuang, *Physics of Photonic Devices* (John Wiley & Sons, New York, 2009).
[47] F. O. Afzal, S. I. Halimi, and S. M. Weiss, J. Opt. Soc. Am. B, JOSAB **36**, 585 (2019).
[48] D. Rosser, T. Fryett, A. Saxena, A. Ryou, and A. Majumdar, Opt. Mater. Express **10**, 645 (2020).
[49] E. W. Martin, J. Horng, H. G. Ruth, E. Paik, M.-H. Wentzel, H. Deng, and S. T. Cundiff, Phys. Rev. Appl. **14**, 021002(R) (2020).
[50] S. Kang, K. Kim, B. H. Kim, J. Kim, K. I. Sim, J.-U. Lee, S. Lee, K. Park, S. Yun, T. Kim, A. Nag, A. Walters, M. Garcia-Fernandez, J. Li, L. Chapon, K.-J. Zhou, Y.-W. Son, J. H. Kim, H. Cheong, and J.-G. Park, Nature (London) **583**, 785 (2020).
[51] L. C. Andreani, G. Panzarini, and J.-M. Gérard, Phys. Rev. B **60**, 13276 (1999).
[52] G. Panzarini and L. C. Andreani, Phys. Rev. B **60**, 16799 (1999).
[53] L. C. Andreani, *Strong Light-Matter Coupling* (World Scientific, Singapore, 2013), pp. 37–82.
[54] S. Fan, Ş. E. Kocabaş, and J.-T. Shen, Phys. Rev. A **82**, 063821 (2010).
[55] E. Rephaeli and S. Fan, IEEE J. Sel. Top. Quantum Electron. **18**, 1754 (2012).